Supplementary Information (SI) for Chemical Science.

A Bioimmune Mechanism-inspired Targeted Elimination Mechanism on Anode Interface Towards Zinc-iodine Batteries

Kaixin Wang[a], Yuting He[a], Ruduan Yuan[a], Zhaoyu Chen[a], Qianzhi Gou[a,b], Sida Zhang[a], Huaping Mei[b], Yujie Zheng[a], John Wang[c,d], Meng Li[a]*

a. National Innovation Center for Industry-Education Integration of Energy Storage, MOE Key Laboratory of Low-grade Energy Utilization Technologies and Systems, *CQU-NUS* Renewable Energy Materials & Devices Joint Laboratory, College of Energy & Power Engineering, Chongqing University, Chongqing 400044, China.

b. School of Building Services Science and Engineering, Xi'an University of Architecture and Technology, Xi'an, 710055, China

c. National University of Singapore (Chongqing) Research Institute, Chongqing 401123, China

d. Department of Materials Science and Engineering, National University of Singapore, Singapore, 117573

**Corresponding author: limeng@cqu.edu.cn (Dr. M. Li)*

Keywords: Aqueous Zinc-ion Batteries; Electrolyte; Zn Anode; Elimination; By-product

EXPERIMENTAL SECTION

Synthesis of Cy-H and HCl.

A baseline electrolyte of 2 mol L^{-1} ZnSO4 was prepared by dissolving Zinc sulfate ($ZnSO_4 \cdot 7H_2O$, AR, Macklin) in deionized water. Cysteamine hydrochloride (C_2H_8ClNS) was added to the prepared 2 mol L^{-1} $ZnSO_4$ electrolyte to obtain 0.01 M Cy-H electrolytes. hydrochloric acid (HCl) was added to the prepared 2 mol L^{-1} $ZnSO_4$ electrolyte to obtain 0.01 M HCl electrolytes.

Fabrication of I_2 cathode materials.

Firstly, 50 mg of activated carbon and 50 mg of iodine particles were dissolved in 500 ml of water and sonicated for 2 h. Then, the solution was stirred at room temperature for 48 h. Then, a centrifuge was used at a speed of 8000 rmp for 10 minutes, and the above steps were repeated five times. The obtained solid-liquid mixture was freeze-dried for 12 h to obtain a positive electrode active material sample. The cathode materials are composed of I_2, conductive super-P and PVDF at a mass ratio of 7:2:1 in N-methyl pyrrolidone solvent. Then, the slurry mixture was coated on the Ti foil and dried in 80°C overnight in a vacuum oven and then cut into discs of 14 mm diameter (mass loading of 0.8-1.0 mg cm^{-2}).

Materials Characterization

The Nuclear magnetic resonance (NMR) spectra were recorded on a Bruker Avance NEO 400 MHz instrument. The PerkinElmer Lambda 365+ was adopted to record the concentration change of Cy-H and HCl additives before and after cycles. Scanning electron microscopy (SEM, Zeiss Auriga SEM-FIB) On a Bruker D2 Phaser X-ray diffractometer (XRD) with Cu-Kα radiation (λ=1.54178 Å) ranging from 10 to 80° the phase structures of samples were charactered. The XPS (Thermo ESCALAB 250XI) with an Al Kα radiation source was applied to explore the elemental composition and the valence state of the as-prepared samples. The SuperViewW1 (CHOTEST) is used to measure the surface morphology of the electrode.

Theoretical Calculations

We used density functional theory to perform ESP calculation, B3LYP combined with 6-31G base set, and opt+freq to analyze the model, so that the optimized geometric structure has no virtual frequency. Finally, VMD+MULTIWFN was used to output the results. In this study, the molecular dynamics simulations were performed using the LAMMPS software package, and all systems were simulated under the Lennard-Jones potential field. The SPC/E water model was used for the water molecules and the simulation box was constructed by MOLTEMPLATE software. The dimensions of the simulation system were 60 Å × 60 Å × 60 Å and contained a total of 7770 molecules. During the simulation, the carbon wall was immobilized and the system was operated under the NVT system, with the temperature maintained at 300 K and controlled by a Nosé-Hoover thermostat. The entire system was simulated for 10 ns with a time step of 1 fs. The model was visualized using OVITO software and the simulation results were processed and analyzed using Visual Molecular Dynamics (VMD) software.

Electrochemical measurements.

The CR2032-type coin cells composed of various electrodes, glass fiber separator (GF/D, Whatman), and 2 M $ZnSO_4$ aqueous electrolyte were assembled to evaluate the electrochemical performance various type coin cells in the air atmosphere. Concretely, symmetric cells were assembled by Cy-H and HCl electrolyte. In order to determine the reversibility of Zn deposition, asymmetric cells were developed using Cy-H and HCl electrolyte and Zn plates as working electrodes, respectively. Full cells were assembled to evaluate the practical feasibility of Cy-H and HCl electrolyte. The as-prepared I_2 electrode is applied as cathode. All full cells were assembled to CR2032 coin cell with Cy-H, HCl and $ZnSO_4$ aqueous solution. Galvanostatic charge/discharge cycling tests were carried out on the NEWARE battery test system. Chronoamperometry (CA), electrochemical impedance spectra (EIS), linear sweep voltammetry (LSV), differential capacitance (DC), and cyclic voltammetry (CV) tests were carried on a Bio-logic electrochemical station. The corrosion current was calculated from Tafel fit system in electrochemical workstation.

Finite Element Analysis (FEA).

In the anode unit of a Zn||Zn symmetric cell, the phase field variables satisfy the Butler-Volmer equation and also comply with the following equations:

$$\frac{\partial \xi}{\partial t} = -L_\sigma \left(g'(\xi) + f_{\mathrm{grad}}^{'}(\xi) + f_{\mathrm{els}}^{'}(u,\xi) \right) - L_\eta h'(\xi) \left(\mathrm{e}^{\frac{(1-\alpha)F\eta}{RT}} - \frac{c_{Zn^{2+}}}{c_0} \mathrm{e}^{\frac{-\alpha F\eta}{RT}} \right)$$

Where ξ (electrolyte, $\xi = 0$; zinc metal anode, $\xi = 1$); L_σ is the interface mobility; L_η is the reaction constant; α and $1-\alpha$ are the charge transfer coefficients; c0 is the initial concentration of the electrolyte; $H(\xi) = \xi^3(6\xi^2-15\xi+10)$ is the interpolation function; $\eta = \varphi_{Zn}-\varphi_e-E_{eq}$ is the overpotential, where φ_{Zn} is the potential of the zinc metal anode, φ_e is the potential of the electrolyte, and E_{eq} is the potential at the electrochemical reaction equilibrium.

The evolution of $c_{Zn}{}^{2+}$ in the electrolyte can be described using the Nernst-Planck equation:

$$\frac{\partial c_{\mathrm{Zn}^{2+}}}{\partial t} = \nabla \cdot \left(D_{\mathrm{Zn}^{2+}} \nabla c_{Zn^{2+}} + D_{\mathrm{Zn}^{2+}} c_{Zn^{2+}} \frac{F}{RT} \nabla \phi_{\mathrm{e}} \right) - c_{\mathrm{Zn}} \frac{\partial \xi}{\partial t}$$

Where $D_{Zn}{}^{2+}$ is the diffusion coefficient of Zn^{2+}, and c_{Zn} is the initial concentration at the electrode.

Geometry structure:

The model proposes a coupled mechanical-electrochemical phase field approach to replicate the multi-physics processes in the anodic half cell of the Zn||Zn symmetric cell. The two-dimensional domain used consists of an electrode with Zn metal nucleation sites and an electrolyte. The initial geometry structure is depicted in the following figure, where the electrolyte is in liquid form.

Model assumptions:

Neglect the opposing cathode where zinc stripping reactions occur; Assume the electrolyte is a concentration constant bulk solution; Due to the electrolyte being either flowable or deformable, assume the Zn-electrolyte interface is in perfect contact after battery encapsulation.

Boundary conditions:

In the anod unit of the Zn||Zn symmetric cell, a constant voltage of 50 mV is applied as the driving force; The boundary load on the upper boundary of the anodic unit in the Zn||Zn symmetric cell is set to 5×10^{-6} Pa; The surface of blocks (representing $ZnSO_4(OH)_6$) do not carry charge.

Model parameters:

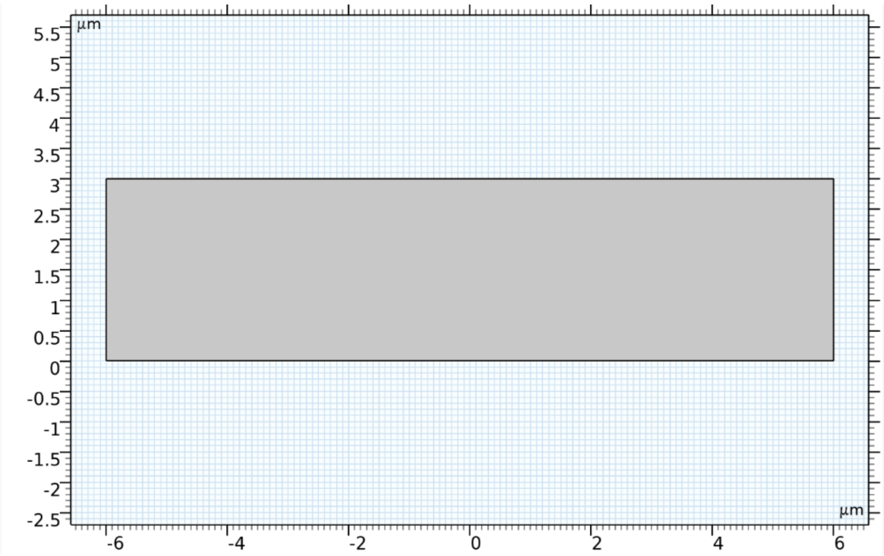

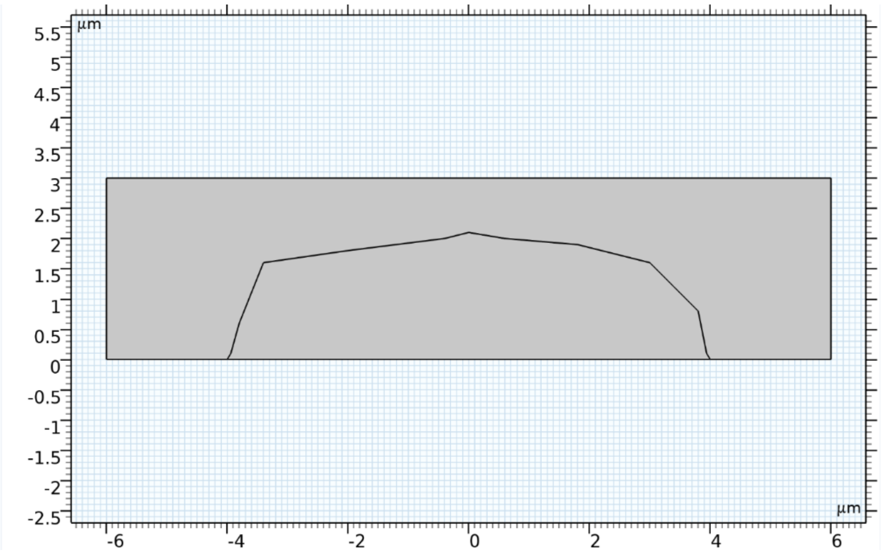

The parameters required for the calculation of the anode unit model in a Zn||Zn symmetric cell are shown in Tab. S1

The pouch cell fabrication process:

The pouch cell fabrication process was meticulously carried out following a standardized protocol. Prior to assembly, precise dimensional specifications were applied to both the Zn foil anode and titanium-platinum coated cathode materials, with corresponding dimensions maintained for the separator membrane. The assembly procedure involved sequential stacking of the cell components in the configuration of cathode-separator-anode, ensuring proper alignment and orientation. Subsequently, the stacked components were carefully inserted into the pouch, followed by the controlled addition of 1000 μL electrolyte to achieve optimal separator wetting. Final encapsulation was performed using a vacuum sealing machine to ensure proper cell integrity and prevent electrolyte leakage. The accompanying schematic illustration provides a detailed representation of the internal architecture and component arrangement within the fabricated pouch cell.

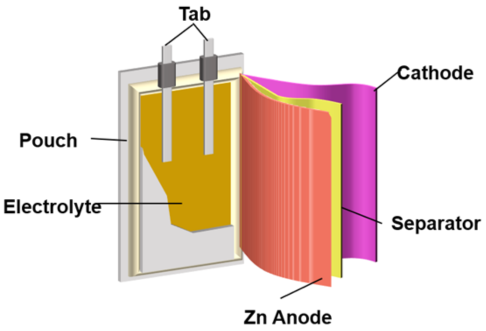

Test Details About Differential Electrochemical Mass Spectrometry (DEMS).

The relationship between HER reaction intensity and electrolyte ph value：

A three-electrode system was used for the test. The working electrode consisted of a gold film, while a titanium wire served as the counter electrode, and an Ag/AgCl electrode was utilized as the reference. Continuous hydrogen evolution reactions were conducted at a constant current density of 5 mA cm^{-2} in electrolytes with varying acidity levels. The acidic electrolytes were prepared by adding hydrochloric acid (HCl) to a 2 M zinc sulfate (ZSO) solution.

Hydrogen precipitation test procedure for symmetric cells:

The hydrogen evolution evaluation for symmetric cells was conducted following a standardized protocol. Symmetric Zn-Zn cells were fabricated using a specialized assembly mold, incorporating GF-D as the separator membrane. Electrolyte solutions (ZSO and Cy-H) were precisely introduced via controlled dropwise addition. Prior to electrochemical characterization, the assembled cells underwent a 4-hour stabilization period under nitrogen atmosphere to ensure establishment of internal equilibrium. The hydrogen evolution assessment was then performed using an electrochemical workstation, employing a constant current density of 5 mA cm^{-2} for zinc deposition/stripping measurements. Throughout the experimental procedure, a nitrogen environment was maintained to prevent atmospheric interference.

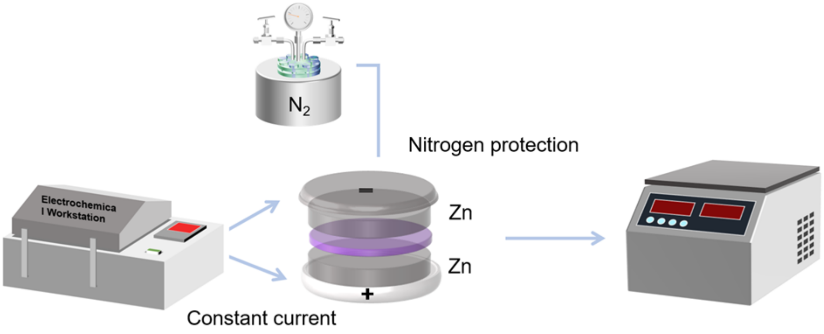

Tab. S1 Model parameters required for the calculation

Structural parameter	**Height (μm)**	**3**
	Width (μm)	**12**
Physical parameter	**Ambient temperature (K)**	**298.15**

	Electrolyte diffusion coefficient (m^2/s)	**2×10^{-15}**
	Electrode diffusion coefficient (m^2/s)	**2×10^{-15}**
Material parameters	**Conductivity of zinc metal (S/m)**	**0.16×10^{-7}**
	Zinc metal measuring point density (mol/m^3)	**109667**
	Electrolyte conductivity (S/m)	**0.1**
Operation parameters	**Electrochemical reaction rate constant (1/s)**	**0.5**
	Interface migration rate ($m^3/(J*s)$)	**10^{-6}**
	Initial electrolyte concentration (mol/L)	**1**

Figure Section:

SI 1. Molecular formula of Cy-H.

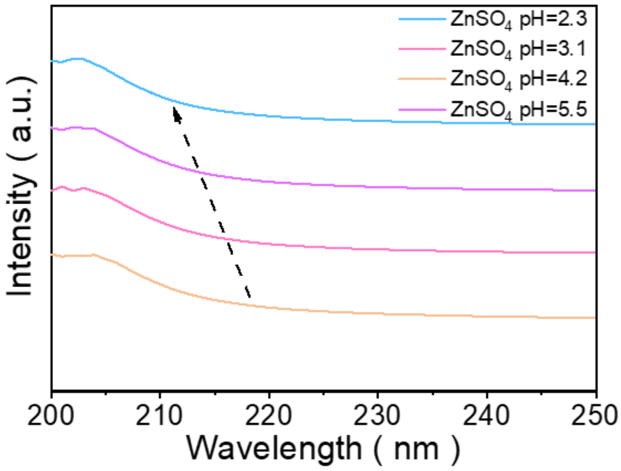

SI 2. UV-vis spectra of various electrolytes.

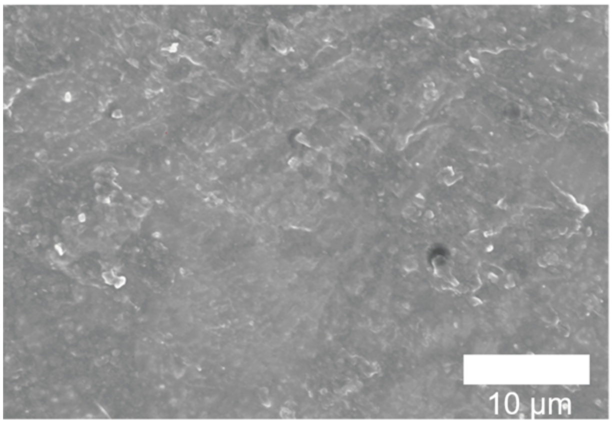

SI 3. SEM of the electrode after immersion in Cy-H.

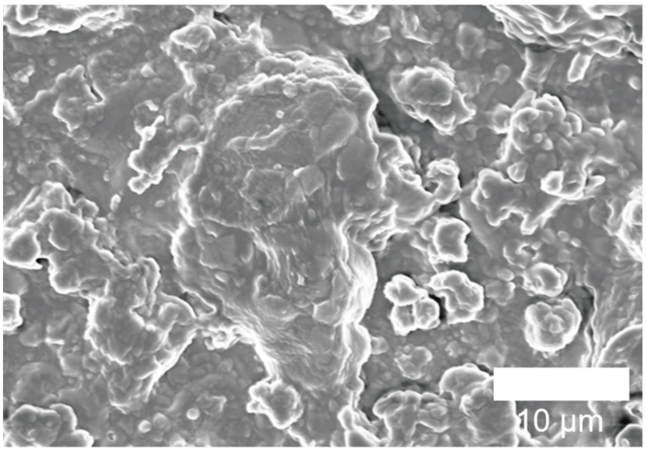

SI 4. SEM of the electrode after immersion in ZSO.

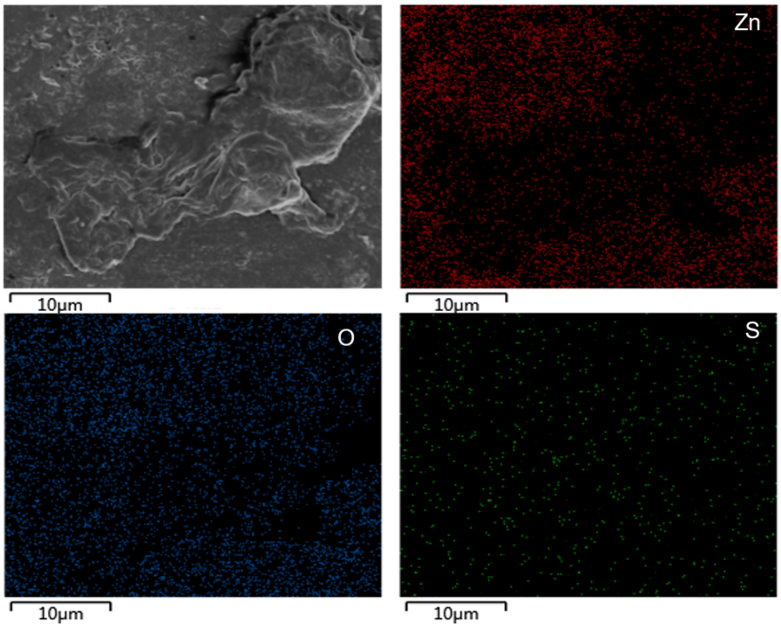

SI 5. EDS mapping of Zn anode after $ZnSO_4$ electrolyte immersion.

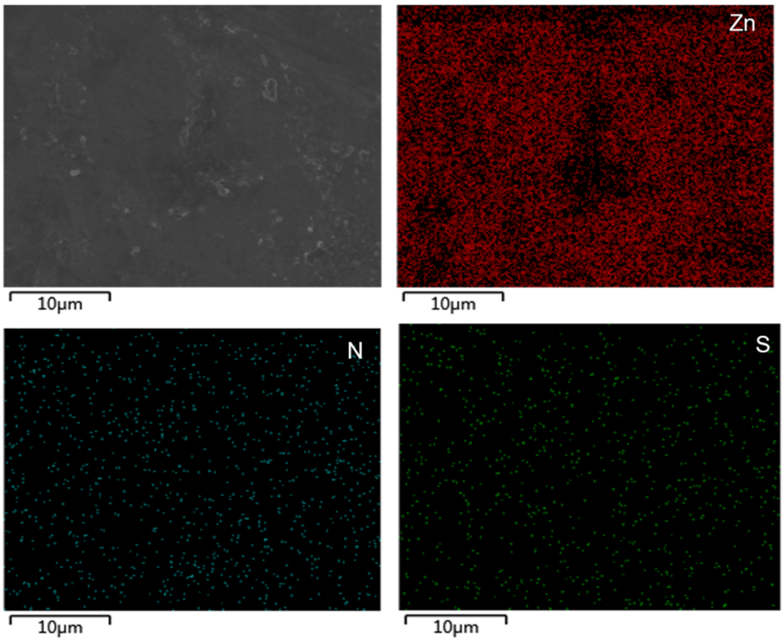

SI 6. EDS mapping of Zn anode after Cy-H electrolyte immersion.

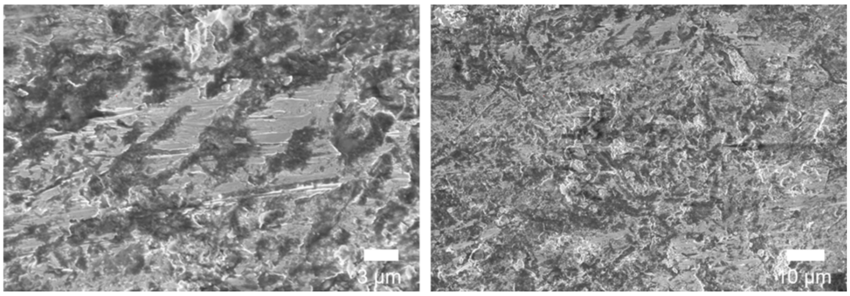

SI 7. SEM images of Zn anode after HCl electrolyte immersion.

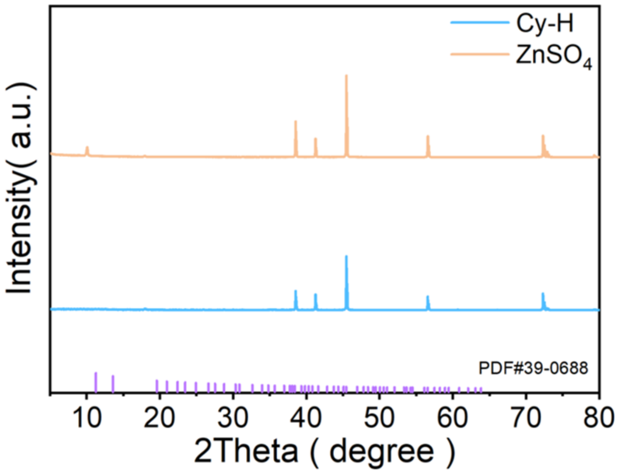

SI8. XRD spectra of Zn anode after immersion.

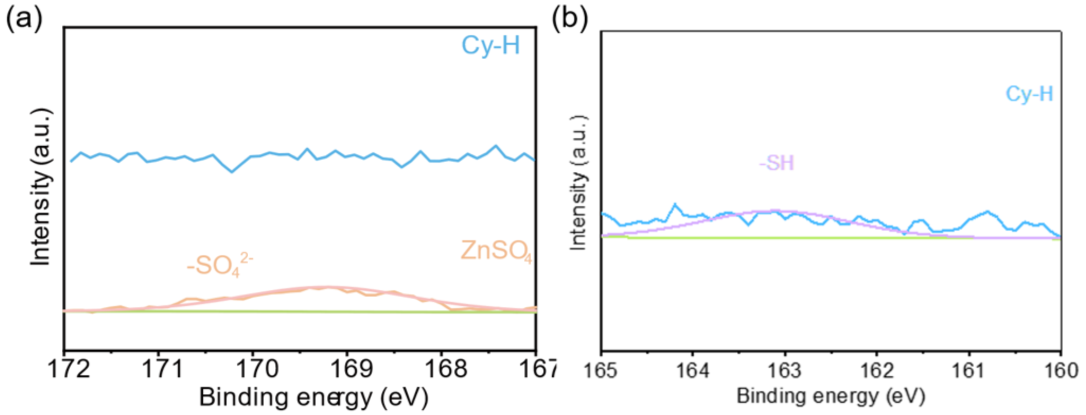

SI 9. S2p XPS spectra of the Zn anode after immersion.

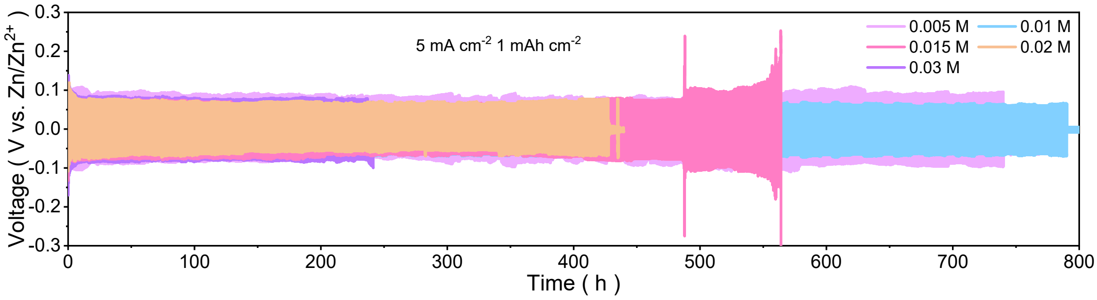

SI 10. Voltage profiles of Zn//Zn symmetric cells at 5 mA cm^{-2}.

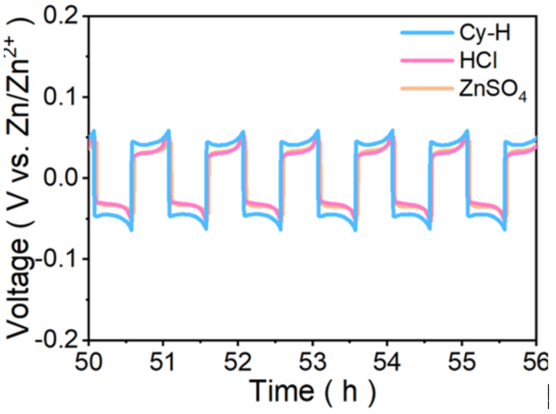

SI 11. Voltage profiles of Zn||Zn symmetric cells at 0.5 mAh cm^{-2}.

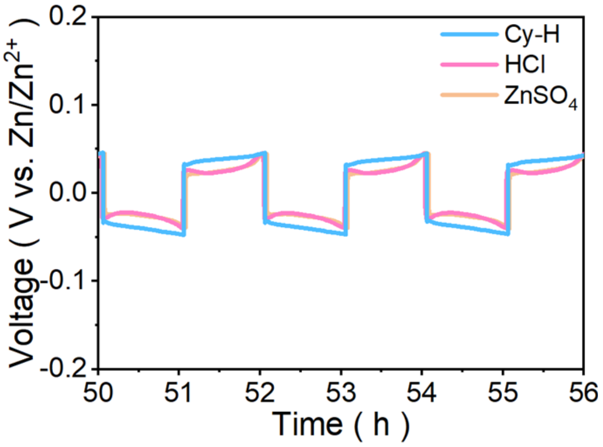

SI 12. Voltage profiles of Zn||Zn symmetric cells at 1 mAh cm^{-2}.

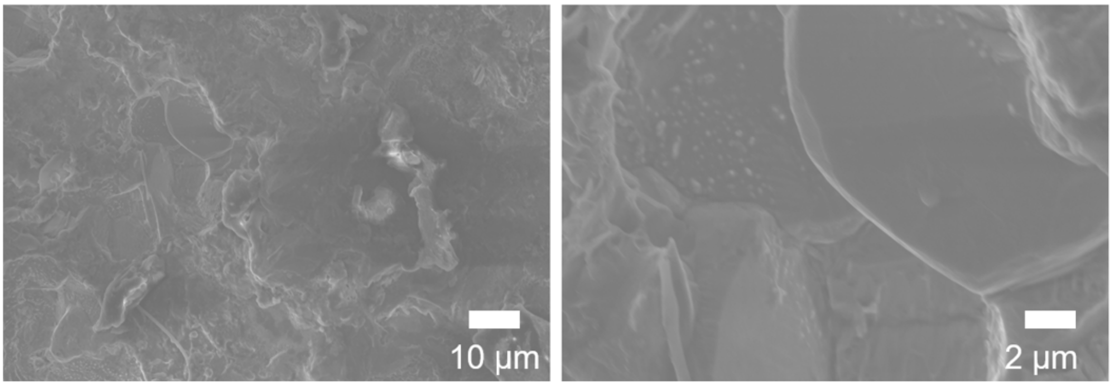

SI 13. SEM image of Zn anode electrode after Cy-H cycling.

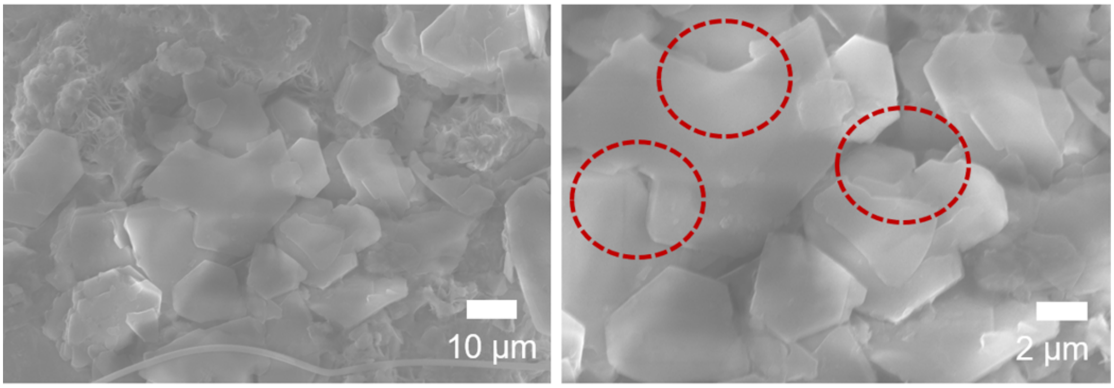

SI 14. SEM image of Zn anode electrode after HCL cycling.

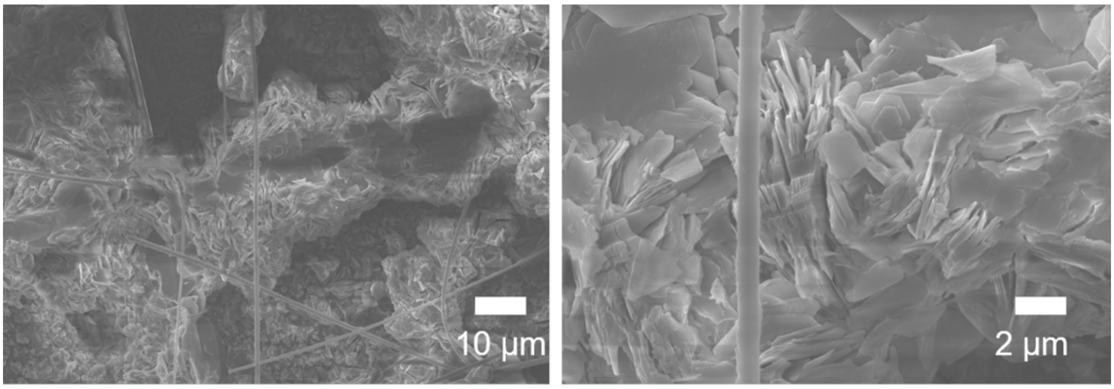

SI 15. SEM image of Zn anode electrode after $ZnSO_4$ cycling.

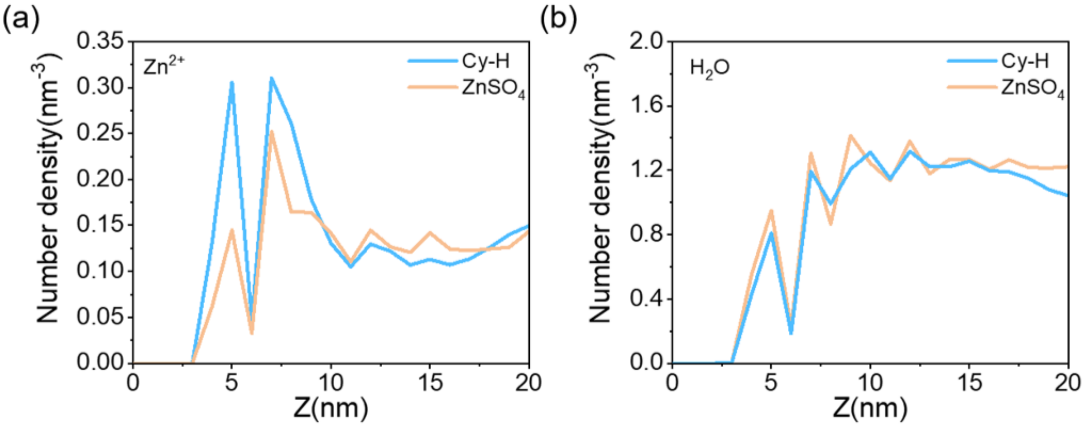

SI 16. Corresponding distribution in the Cy-H electrolyte obtained by MD simulation.

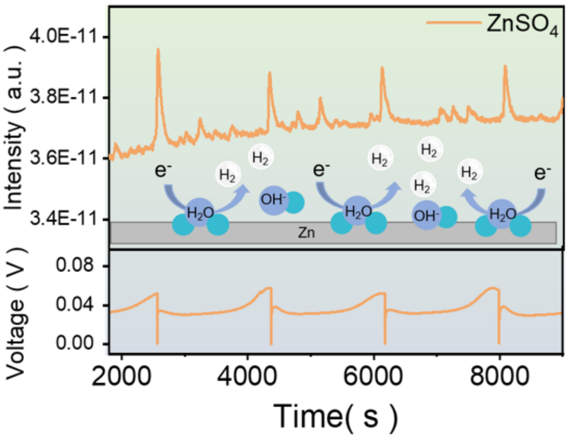

SI 17. DEMS test pattern of $ZnSO_4$.

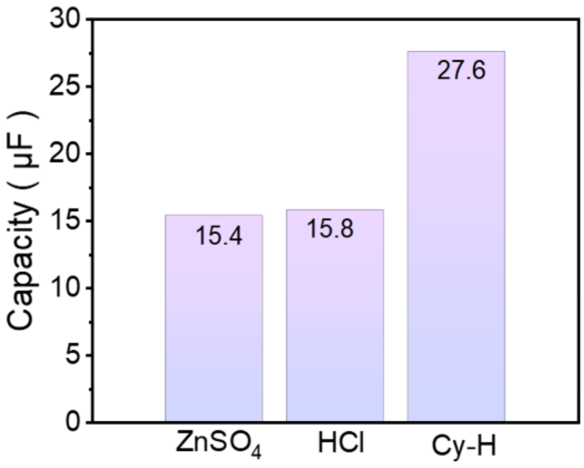

SI 18. EDL capacitance results obtained from EIS testing.

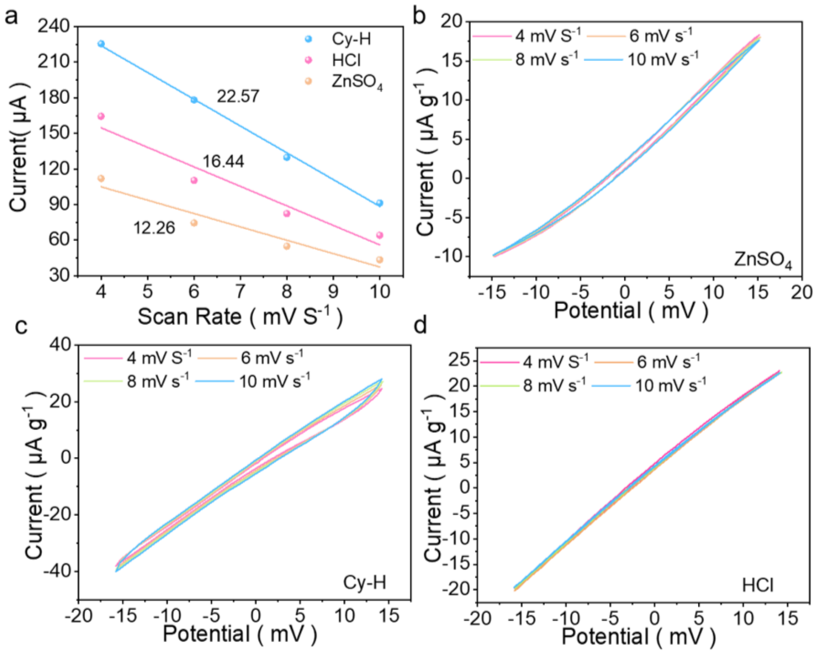

SI 19. EDL capacitance results obtained from CV.

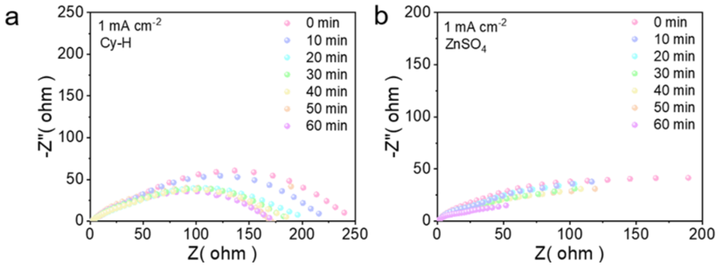

SI 20. In-situ EIS spectra of Cy-H a) and $ZnSO_4$ b).

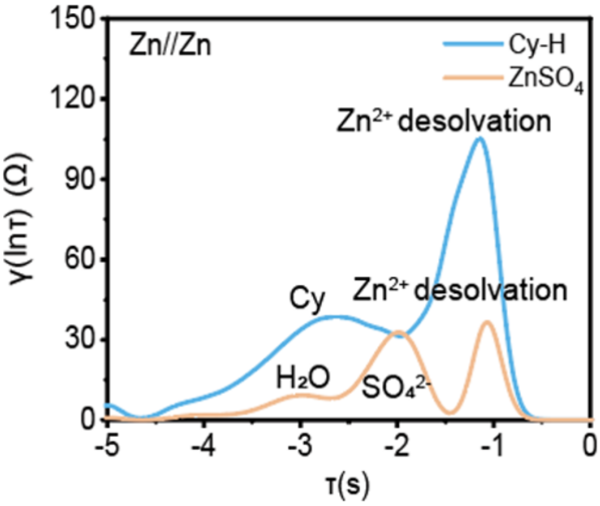

SI 21. DRT spectra of Cy-H.

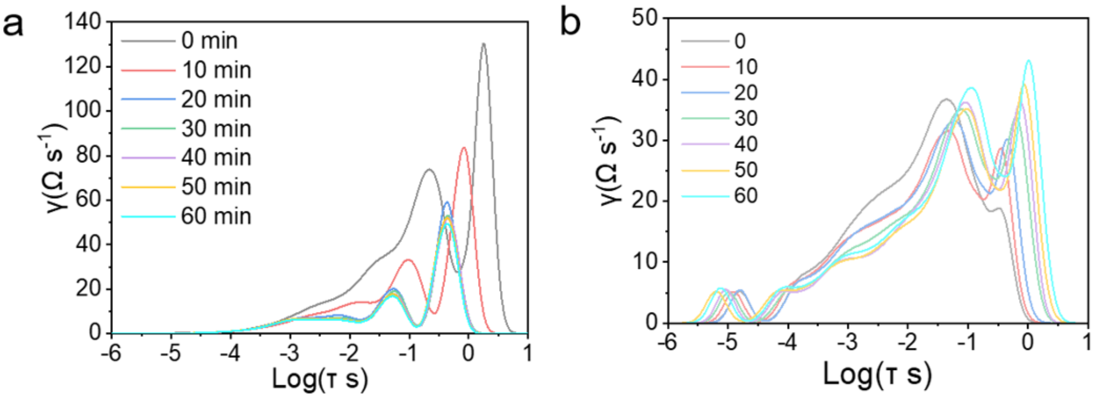

SI 22. In-situ DRT spectra of Cy-H a) and $ZnSO_4$ b).

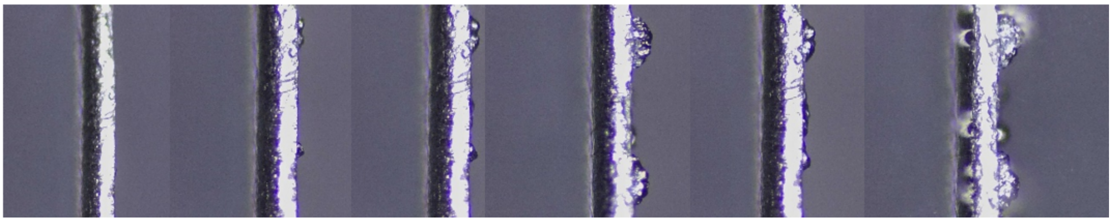

SI 23. In–situ optical images of the Zn plating on Zn anode in $ZnSO_4$.

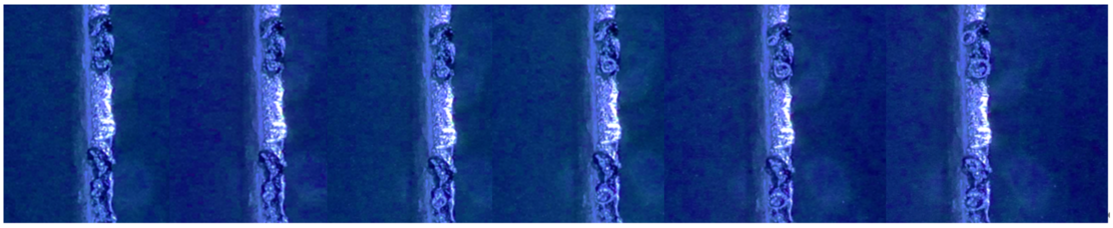

SI 24. In–situ optical images of the Zn plating on Zn anode in HCl.

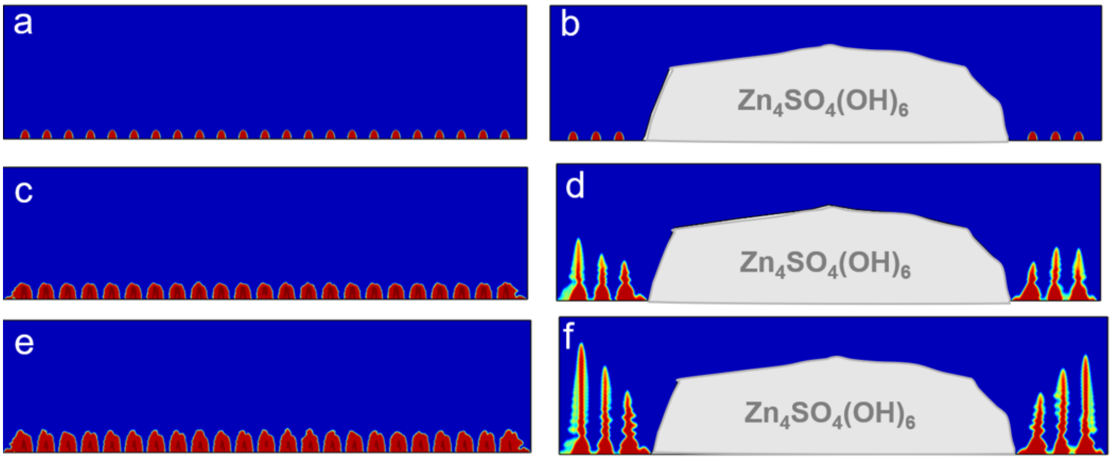

SI 25. Morphology of Zn dendrite growth at 0 s a-b), 60 s c-d), 90 s e-f).

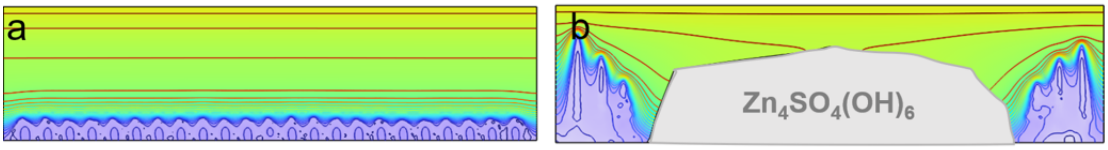

SI 26. Electric field intensity distribution of Zn dendrite growth at 60 s.

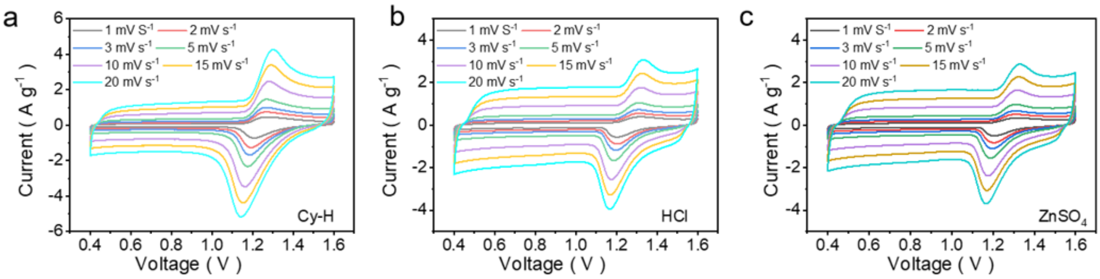

SI 27. CV curves of Zn//I_2 full cells at different scan rate with different electrolyte.

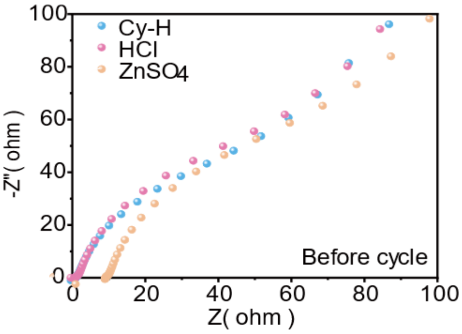

SI 28. EIS of Zn//I2 full cells with different electrolytes

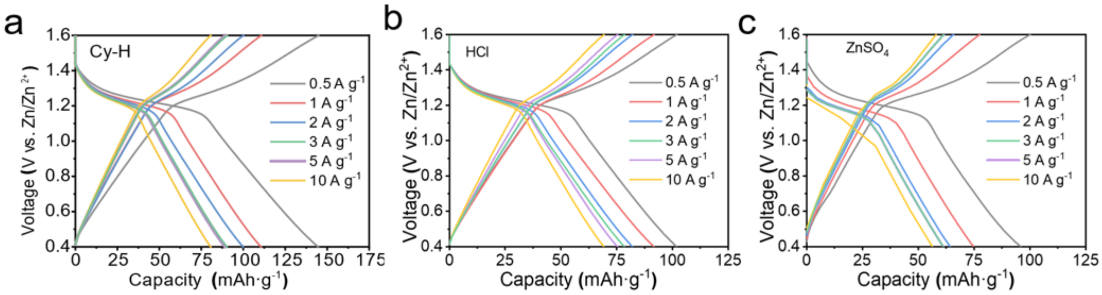

SI 29. charge/discharge voltage profiles of a) Cy-H, b) HCl and c) $ZnSO_4$.

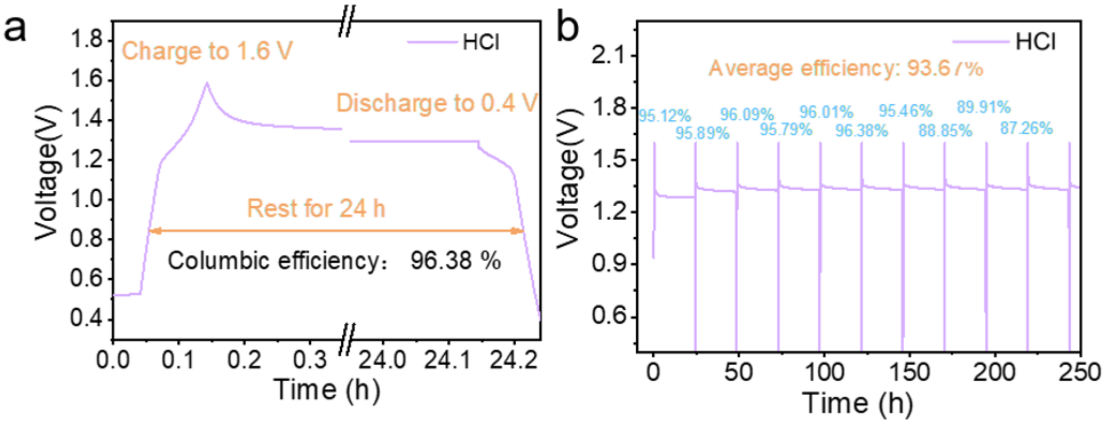

SI 30. Self-discharge a) and ten consecutive self-discharge tests b).

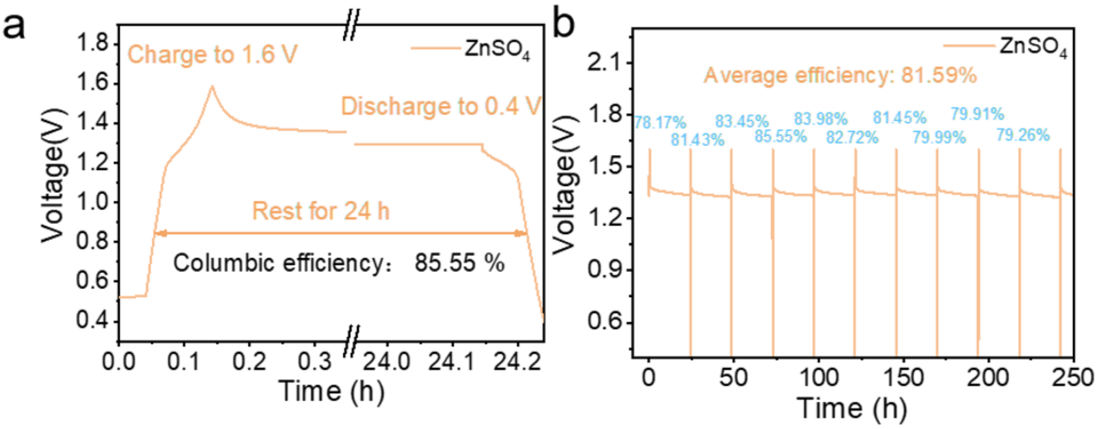

SI 31. Self-discharge a) and ten consecutive self-discharge tests b).

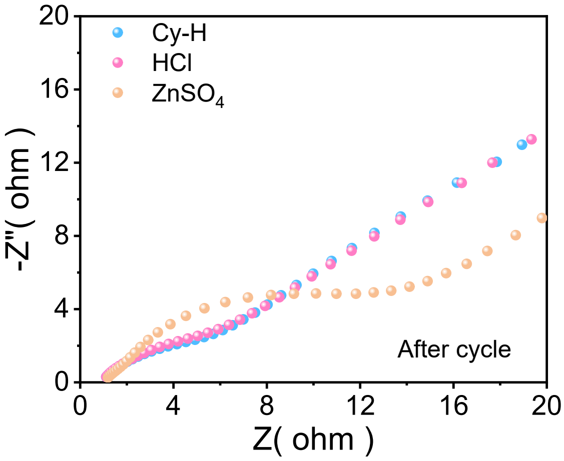

SI 32. EIS plots of the full cell after cycling.

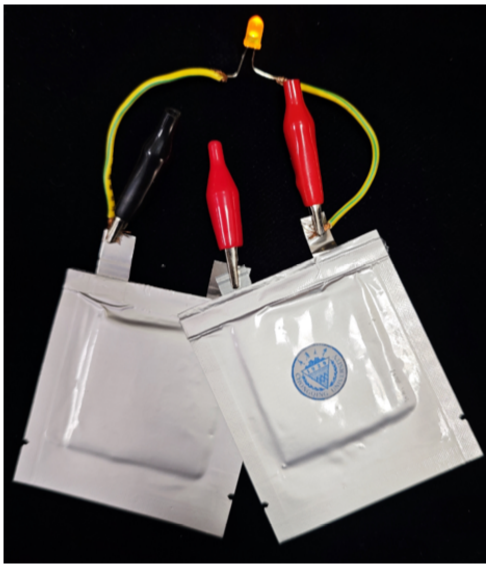

SI 33. pouch battery powering a small light bulb.

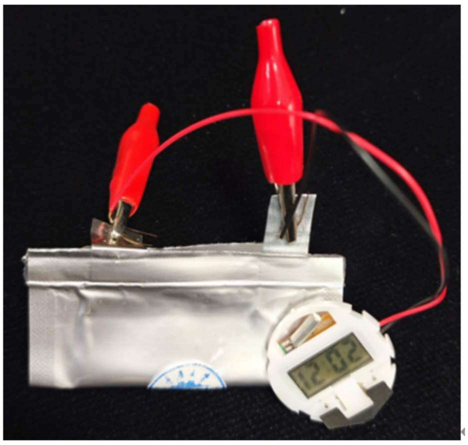

SI 34. pouch battery powering a watch in bending state.

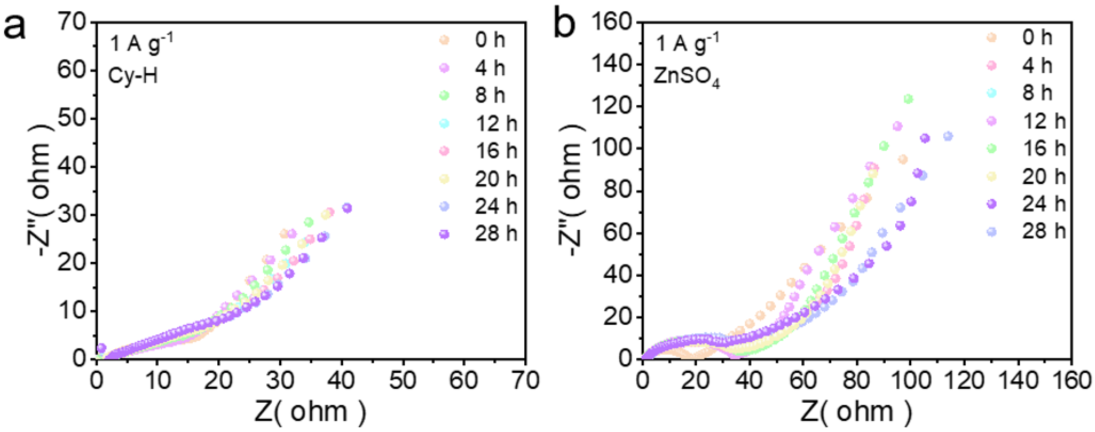

SI 35. In-situ EIS plots during self-discharge of Cy-H a) and $ZnSO_4$ b).

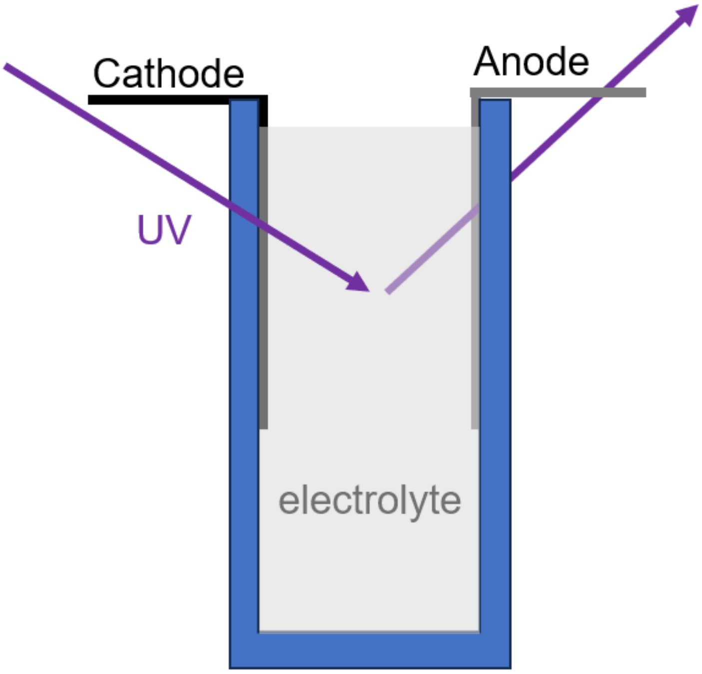

SI 36. Self-built in-situ UV observation device.